Flowing damage in ion-implanted amorphous silicon

Jean-Christophe Pothier, François Schiettekatte, and Laurent J. Lewis*

Département de Physique et Regroupement Québécois sur les Matériaux de Pointe (RQMP), Université de Montréal, Case Postale 6128, Succursale Centre-Ville, Montréal, Québec, Canada H3C 3J7

(Received 7 October 2010; revised manuscript received 10 February 2011; published 9 June 2011)

Using molecular-dynamics simulations, we have studied the creation and evolution of damage in crystalline and amorphous silicon following the implantation of energetic keV ions. A method is proposed to identify anomalous atoms based on a weighted combination of local, atomic-scale properties, which applies to both Si phases. For crystalline Si, the passage of the ions causes compact amorphous regions to form, while no evidence for melting is observed. The relaxation of the amorphouslike regions proceeds initially by the rapid recrystallization of smaller clusters and isolated atoms, followed by a long period of steplike changes in the number of defects due to spontaneous annealing of damage pockets at the crystalline-amorphous interface. In amorphous Si, the initial stage of damage annealing (which lasts a few picoseconds) resembles closely that observed in crystalline Si; on larger time scales, however, the damage is found to "percolate," or flow, through the system, inducing damage away from the collision cascade, thus causing an overall "derelaxation" of the material.

DOI: 10.1103/PhysRevB.83.235206 PACS number(s): 61.80.Az, 78.20.Bh

I. INTRODUCTION

Ion implantation produces complex damage structures in semiconductors. In monocrystaline silicon (*c*-Si), accumulated damage is responsible for such phenomena as enhanced diffusion of dopants, eventually taking the material to a new phase, viz., amorphous silicon (*a*-Si). Many experiments, as well as molecular-dynamics (MD) simulations, have shown that, for the most part, the structures resulting from keV ion impacts in *c*-Si consist of metastable defect clusters referred to as "amorphous pockets."[1–5] The situation—the damage resulting from ion impacts—would be expected to be very different in *a*-Si given the difference of the initial structures but, interestingly, temperature annealing leads to similar calorimetric signals in both implanted materials.[6,7] Indeed, *a*-Si shares with *c*-Si a number of physical characteristics, namely, an averaged atomic coordination close to 4, an averaged bond angle close to the ideal tetrahedral value, and a similar nearest-neighbor distance.[8] It is therefore tempting to compare the structural evolution in both phases of the material, namely, by examining the annealing of the damage that follows implantation. However, implantation damage cannot be easily identified in *a*-Si, either experimentally or from computer models. We aim in this work at comparing the evolution of damage in the two systems, and this requires removing, at least partially, the difficulties inherent to the definition of damage in computer-simulated *a*-Si.

In models of *c*-Si, Diaz de la Rubia and Gilmer[5] have shown that the amorphous pockets anneal in a stepwise manner, often involving tens of atoms at the surface of the pockets. They also found that the structure of the cascade regions forming along the path of the energetic ions is similar to that of liquid silicon (coordination number ∼6.5) for about 2 ps after implantation, after which it quickly restructures into *a*-Si (coordination number ∼4.3). Similar results have been obtained by Santos *et al.*[9] for 1 keV ion-implanted *c*-Si targets; they found that while 25% of the damage are point defects, 75% belong to *a*-Si clusters varying in size from a few atoms to more than 50. Likewise, Caturla *et al.*,[10] using criteria based on energy and bond-angle variations,[11] observed the formation of structures resembling *a*-Si which recrystallize in a stepwise way and which appear to be characteristic of the evolution of these pockets. Such a behavior, observed by microscopy experiments,[12] was presumed to be responsible for the broad features of the heat release curve in nanocalorimetry experiments.[7] A similar behavior was observed in ion-implanted *a*-Si but with a larger heat release, suggesting that the annealing mechanisms are similar in *a*-Si and *c*-Si but that the structure surrounding the damage clusters plays an important role in damage formation and annealing dynamics.[7]

In order to assess more closely a possible correspondence with *c*-Si, it is necessary to be able to follow the evolution of implantation damage in *a*-Si. Various approaches have been proposed to identify defects in this material. Among others, using tight-binding MD simulations, Urli *et al.* have observed a strong correlation between charge and volume for point defects, i.e., vacancies and interstitials.[13] Also, Kim *et al.* have shown using an *ab initio* approach that vacancies can be stable for up to 10 ps at room temperature, for any defect concentration.[14] Thus, in principle, it appears to be possible to locate point defects with some precision in *a*-Si and follow their evolution. These methods are, however, based on computational approaches which are much too demanding for the large systems required here to accommodate the extensive damage resulting from energetic-ion implantation cascades.

In the present work, we propose a method for locating implantation damage in MD-simulated amorphous materials using much faster empirical potentials. The idea is to identify "anomalous atoms" by determining how far their properties lie from the average (or "normal") characteristics of the material. Evidently, the method also applies to crystalline materials, where anomalous atoms should be found at locations close to topological defects, which are easy to identify. By applying it to both *a*-Si and *c*-Si, we are able to characterize the evolution of the implantation damage in the two materials following the ion impacts. The results are remarkable: while the behaviors of the two materials are very similar in the early stages of damage production and evolution, very significant differences appear

on longer time scales (over a picosecond or so). While *c*-Si relaxes in a stepwise manner, as mentioned above, *a*-Si anneals smoothly; the damage is found to "percolate," or flow, through the system, causing an overall "derelaxation": damage spreads away from the collision cascade, a larger number of atoms being affected than in the early stage of damage production but each closer to the ideal amorphous state so that the total energy decreases, i.e., the system effectively relaxes. Before presenting our results, we first discuss the computational framework we have used; the tools for analyzing the simulated samples, and in particular the damage following implantation, are discussed in Sec. III.

II. COMPUTATIONAL DETAILS

A. MD simulations and models

We model the interactions between atoms using the Stillinger-Weber (SW) potential,[15] properly modified with the two-body Ziegler-Biersack-Littmark potential[16,17] to account for short-range interactions that occur upon the passage of energetic ions. The SW potential has demonstrated its relevance in describing various configurational properties of silicon in the crystalline phase as well as in the amorphous and liquid phases.[5,10] This potential is "classical" in the sense that electrons are not explicitly taken into account but, rather, included in an effective way in the potential.

Details of the simulated systems are as follows: the models on which most of our calculations were performed contained 101 568 (*c*-Si) and 100 000 (*a*-Si) atoms, respectively, with corresponding dimensions of $124.9 \times 124.9 \times 130.3$ Å^3 and (124.9 Å)^3; the model for *a*-Si was kindly provided by Mousseau.[18–20] In order to mimic an infinite slab of material, periodic boundary conditions were imposed in the x and y directions, which are parallel to the surface. We also used a variable time step based on the most energetic atom in order to speed up the simulations after most of the energy brought into the system by the implanted ion has dissipated in the bulk; the time step was thus varied between 0.01 and 1 fs. Before implantation, each target was carefully relaxed at room temperature (300 K). For reference, we present in Table I the structural properties of the two duly relaxed models. The coordination number for *a*-Si slightly exceeds 4, but this is a well-known limitation of the SW potential;[18,21–23] this should be of little consequence since we will be comparing states of the system before and after implantation, so that systematic errors largely cancel out. The calculations were carried out using the programs groF, a multipurpose MD code developed by one of the authors (L.J.L.), as well as LAMMPS, an open-source classical MD code.[24]

B. Implantation

In order to simulate the implantation process, Si atoms were placed just above the topmost z plane of each target and given an initial kinetic energy of 3 keV directed toward the surface; the azimuthal angle—the angle between the normal to the surface and the direction of incidence—was varied between 5° and 136° so as to reduce the probability of channeling, evidently quite large in the crystalline targets. The (x, y) positions of the incident atoms were chosen to be in the center of the targets in order to avoid boundary effects. Up to twenty different simulations in *c*-Si and ten in *a*-Si, using different target sizes and implantation angles, were carried out for comparison purposes. To minimize possible interferences between the periodic images of the supercells, as well as artifacts from the finite thickness of the slabs, the outermost 5 Å layer of each side of the simulation box (except the top surface on which the ion impinges) was used as a 300 K Langevin heat bath,[25] thus releasing the excess energy deposited in the material. Thermal equilibrium is achieved on a time scale of about 1 ps.

III. RESULTS

In order to assess the importance and the extent of damage in *a*-Si following the passage of energetic ions, it is important to compare to a well-defined reference—here *c*-Si—in which defects can be easily located. Indeed, the identification of defects in *a*-Si is a difficult problem since the disorder manifests itself on all length scales.[13] The tools that are normally employed in the case of *c*-Si, largely based on the analysis of such local properties as potential energy and bond-angle variations on specific atoms,[5,10,11] are therefore not *a priori* suitable for the amorphous material. As discussed in Sec. III B, we found that the best method applicable to *a*-Si involved a combination of several properties, viz., potential energy, bond-angle distribution, and the coordination number combined to the radial distribution function (RDF), that can be compared to their crystalline counterparts. In the next section, we discuss the identification and evolution of damage in a crystalline target using a "conventional" topological approach; this will serve as reference for benchmarking our method, presented in the subsequent section.

TABLE I. Structural properties of the relaxed models (300 K).

Property	*c*-Si	*a*-Si
Coordination number	4.0	4.149
Nearest-neighbor distance (Å)	2.35	2.37
Position of first minimum (RDF) (Å)	2.93	2.93
Equilibrium energy (eV)	−4.2947	−4.0674
Average bond angle (deg)	109.39	107.72
Standard deviation of bond-angle distribution (deg)	3.25	16.51
Average Voronoï volume (Å^3)	20.068	20.23
Density (g/cm^3)	2.324	2.305

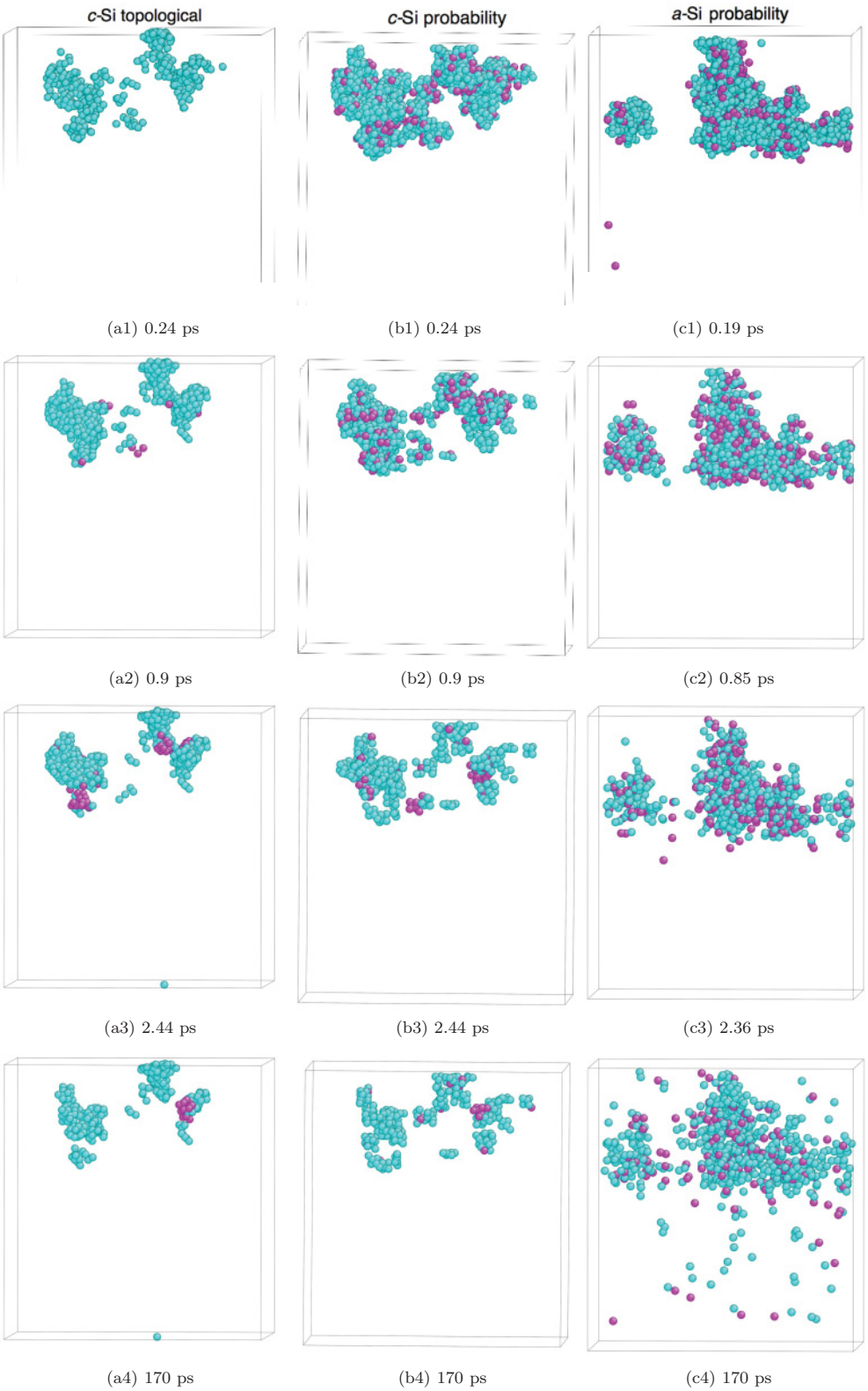

FIG. 1. (Color online) Distribution of defects in *c*-Si (left and center columns) and *a*-Si (right column) at times indicated. Only defective atoms are shown, as identified using the topological method (left column for *c*-Si) or the probability-function method (center column for *c*-Si, right column for *a*-Si). Atoms colored in purple (darker) are those that will return to a normal state within the following few time steps.

A. Crystalline target

In the crystalline material, defects can be identified using a simple topological method which determines whether the structure near a given atom is in a diamondlike environment or not; this is done by verifying the coordination number and analyzing the geometry of the six-atom rings surrounding the atoms.[26,27] On average (based on 20 different "experiments"), a 3 keV Si ion yields about 500 defects distributed in clusters ranging in size from 10 to 200 atoms, an example of which is presented in Fig. 1(a). These results are similar to those obtained by Diaz de la Rubia and Gilmer[5] and Caturla *et al.*[10]

In order to get some indication of the structural character of the damaged regions, we analyzed the clusters of defects in terms of temperature, density, and coordination number, and examined their evolution in time; for statistical significance, we consider here only clusters containing more than ten defects. The density of the clusters rises rapidly to about 2.34 g/cm^3, the coordination number increases to an average of 5.2 and equilibrates back to 4.8 (vs 4 in the perfect crystal) on a time scale of about 1 ps, and the temperature, ∼3500 K 0.2 ps after implantation, drops to ∼1000 K at $t = 1$ ps as the system relaxes. These structural properties do not correspond precisely to those for the amorphous phase (cf. Table I) but, in contrast to earlier results where higher implant energies were considered,[5] are certainly far from the corresponding values for the liquid phase of Si, which has a coordination number in the range 5.8–7 (Refs. 28,29) and density ∼2.57 g/cm^3. In fact, the RDF and the bond-angle distribution suggest that the structure of the clusters is akin to that of a compact *a*-Si phase; indeed, after a few more picoseconds, the coordination number drops to about 4.4 and the density to about 2.296 g/cm^3, quite similar to the values for bulk *a*-Si.

We now discuss the recrystallization process, qualitatively illustrated in the left column of Fig. 1 and quantitatively in Fig. 2. Figure 1(a1) shows the state of the system at $t = 0.24$ ps, corresponding to the maximum in the thermal energy transfer; at this time, the number of defects amounts to about 350, grouped in just a few clusters. Owing to collisions between hot atoms and the rest of the target, the number of defects increases further, reaching a maximum of about 500 at $t = 0.9$ ps (cf. Fig. 2); it then starts to decrease, i.e., recrystallization processes overcome defect generation. Figure 1(a2) shows one such recrystallization process: atoms colored in purple are those defects that will vanish within the following 0.1 ps—these atoms return to the perfect crystalline state. This has been observed in many instances (not shown); the atoms involved are mostly lone defects scattered around in the crystalline structure. The recrystallization process continues until most defects belong to larger clusters.

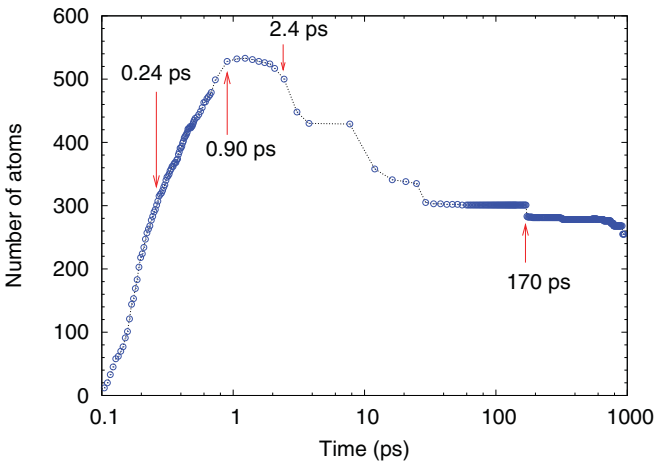

FIG. 2. (Color online) Total number of defects vs time (logarithmic scale) in the crystalline target. The arrows point to the different configurations presented in Fig. 1.

Further relaxation, occurring over much longer time scales, proceeds along another route—through the recrystallization of parts of, or whole, clusters. This is clearly shown in Fig. 2, where the number of defects varies discontinuously, in a stepwise fashion. An example of this is presented in Fig. 1(a3): the purple-colored atoms—56 in total, that is, 11% of the initial number—will recrystallize within the following 0.6 ps. This is the first "large-scale" recrystallization event, and most recrystallization events afterward are of this type: Fig. 1(a4) shows another such event at a much larger time, 168 ps. The 20 purple-colored atoms proceed from an average coordination of 4.5 before recrystallization to exactly 4 after. Overall, Fig. 2 shows that the number of defects drops by 50% in 1 ns.

As can be gathered from the above discussion, the decrease in the number of defects slows down with time as mostly defects with higher activation energies remain: because recrystallization processes are activated, there is progressively less thermal energy available for jumping over the energy barriers leading to the crystalline state. The defective regions that remain, we find, possess a distorted amorphous structure: they are trapped in a local, amorphouslike state, but because they are small, the surrounding crystalline matrix influences their structural and energy properties.

B. Amorphous target

The fact that recrystallization events in implanted *c*-Si usually involve an unpredictable number of atoms, along with the fact that the activation of these events depends on the details of the interface of the damaged region with the crystalline matrix, implies that there should be little or no correlation between the activation energies of such events and the amount of heat released.[30–32] This is the reason for the broad character of the heat release observed in calorimetric measurements.[7] Since a similar behavior is observed in ion-implanted *a*-Si, Karmouch *et al.* suggested that the annealing mechanisms in the two materials are similar.

As discussed earlier, the identification of defects in *a*-Si is much more problematic than in *c*-Si because disorder is everywhere and the topological criteria used above are bound to fail. Nevertheless, in order to get some insight into the initial distribution of implantation damage, some simple analysis can be attempted. For instance, we show in Fig. 3 the distribution of atoms, following the passage of an energetic ion, whose potential energy exceeds −3.25 eV, that is, about 0.8 eV above the equilibrium *a*-Si energy (cf. Table I). This particular value, which has no special meaning, was chosen so as to maximize the number of anomalous atoms belonging to clusters while minimizing the number of lone anomalous atoms—here less than 2%, corresponding approximately to the value found

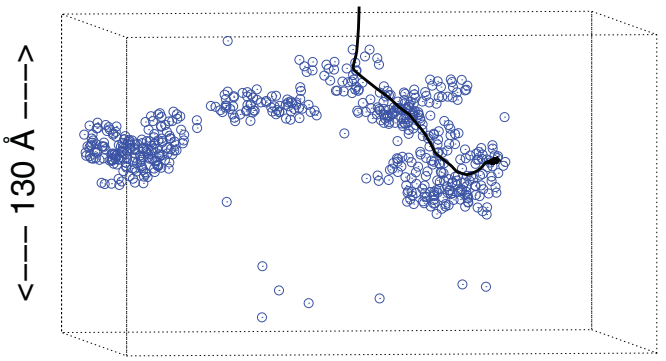

FIG. 3. (Color online) Distribution of atoms whose potential energy exceeds −3.25 eV in the *a*-Si target at $t = 0.2$ ps. The black line indicates the trajectory of the implanted ion.

in the reference crystalline material [Fig. 1(a)]. In fact, the number of atoms above this threshold potential energy is approximately the same as in *c*-Si (and their distributions in space are similar) so that meaningful comparisons between the two systems can be effected.

This approach however is not robust: the atoms rapidly (within a few picoseconds) fall back into the normal distribution of potential energies in *a*-Si, characterized by a (large) standard deviation of about 0.15 eV. Likewise, the usual local structural properties (coordination number, Voronoï volume, nearest-neighbor distances) do not provide the desired criterion by themselves. In fact, it was demonstrated recently, based on a quantum mechanical description of the structure of pure *a*-Si, that point defects could be precisely identified from *cross-correlations* between atomic volume and charge.[13] We thus expect that a proper combination of topological features would provide the desired characterization. In the remainder of this section, we demonstrate that this is indeed the case.

The approach we propose consists in constructing, for each of several topological properties available from the simulations, say x, a "continuous probability" function

$$P(x) = 1 - 1/(1 + e^{(x-x_0)/\sigma_0}), \tag{1}$$

where x_0 and σ_0 are property-dependent adjustable parameters. $P(x)$ provides an estimate of how *anomalous* an atom is (in terms of the particular property x), i.e., how far it is from the relaxed amorphous state, that is, the state defined by averaging over a well-equilibrated, damage-free *a*-Si structure (prepared with the same potential energy function). Thus, a probability of 1 means that the atom is "absolutely anomalous" and a probability of 0 means that it is in a "perfect amorphous state" as defined by the properties listed in Table I. The $P(x)$'s from several physical properties can be combined into a single probability which can then be compared to a reference criterion. In order to provide a solid basis for comparison, this analysis is carried out for both *a*-Si and *c*-Si.

The probability functions we considered, which we chose to be Fermi-like, are detailed in the Appendix. For the potential energy and the bond-angle distributions, the method is straightforward: the value of the property for each atom may simply be compared to the corresponding system-averaged property; this is illustrated in Fig. 4 for the bond angle. Two other properties—the radial distribution function and the

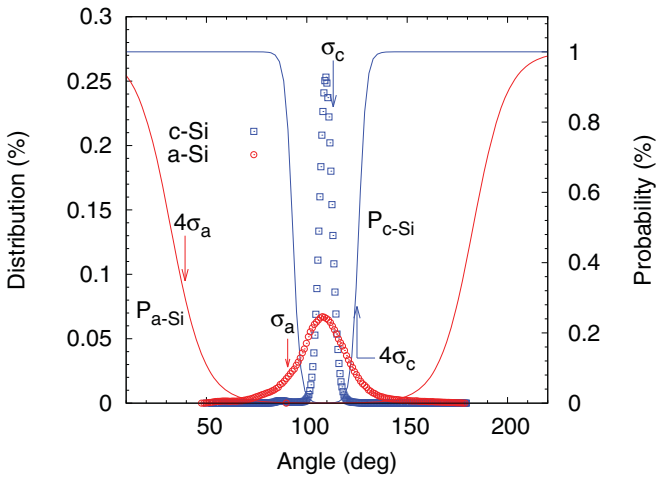

FIG. 4. (Color online) Bond-angle distributions (dots) and probability functions (lines) for both *c*-Si (blue) and *a*-Si (red).

coordination number—were combined into a continuous function; this is discussed in detail in the following section. Note that, because the local properties may fluctuate significantly and rapidly, even in the relaxed amorphous state, much more stable results are obtained by averaging over a few snapshots; we found that averaging over three to six snapshots (up to 0.2 ps) ensures stable results.

1. Coordination number

The coordination number *for a particular atom* is a discrete number so it is not naturally amenable to a continuous description. That being said, the concept of coordination number in disordered materials is somewhat ill defined: it is usually taken as the average number of neighbors within a certain distance from a given atom, normally the minimum between the first- and second-nearest-neighbor peaks in the RDF. Because there is a continuum of possible interatomic distances, and because the identities of neighbors and the corresponding distances change with time, this quantity cannot be defined in an absolute manner; thus bonds can be normal ($r = r_0$, the equilibrium bond distance, 2.37 Å here), tight ($r < r_0$), or loose ($r > r_0$). Recognizing this state of affairs, we may define a distance-dependent, continuous coordination (CC) number for atom i as follows:

$$C_i = e^{k(N-C_p)^2} \sum_j e^{-(r_{ij}-r_0)}, \tag{2}$$

where k is a weight factor, N is the discrete coordination number of atom i (equal to the number of atoms at distance less than the position of the first minimum of the RDF, 2.93 Å–see Table I), and C_p is the coordination number of the ideal system (be it *c*- or *a*-Si), viz., having perfect fourfold coordination; the sum over j runs, in principle, over all other atoms in the system, but in practice only those neighbors at a distance close to r_0 are considered. The prefactor serves as a weight factor which increases the effective coordination number if the atom has too many or too few neighbors. The second factor is a continuous distance-dependent contribution that decreases as neighbors get further away. Thus, in a perfect environment where all (four) neighbors are at distance r_0, $C_i = 4$, exactly.

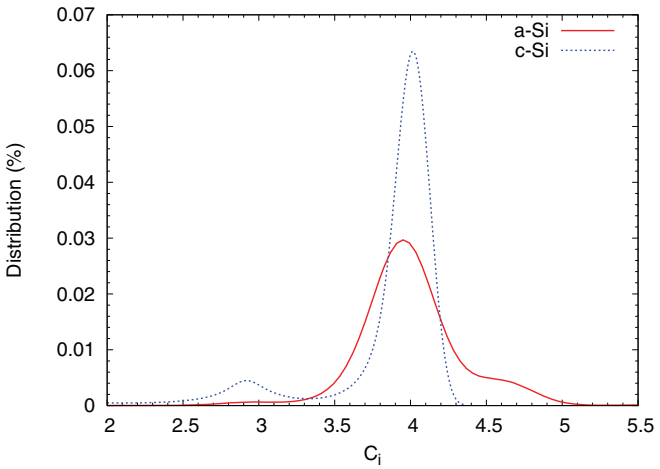

FIG. 5. (Color online) Distribution of the continuous coordination C_i for c-Si and a-Si. The left peak in the c-Si curve is due to surface atoms (which are smoothed out in the a-Si curve).

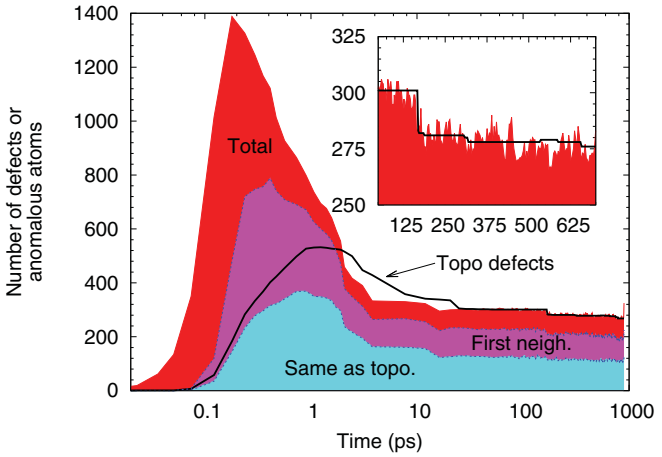

FIG. 6. (Color online) Amount of damage as a function of time in the c-Si target using the probability approach with threshold values of 0.40 and 0.168 (red area) and the topological approach (solid black line). Blue and purple areas correspond to the number of anomalous atoms which are the same as, or first neighbor to, topologically identified defects, respectively.

The distributions of the individual (atomic) values of C_i for our two systems are displayed in Fig. 5. For c-Si, the C_i's are sharply peaked around 4, while the distribution is much broader for a-Si. The probability functions for the occurrence of anomalous atoms, $P(C_i)$, will thus rapidly approach unity as C_i deviates from its normal value.

2. *Atom-specific probabilities*

Because of the inherent disorder in a-Si and the corresponding variations in values of the local properties of the system, we can improve the accuracy of the anomalous atom identification method by defining and referring to atom-specific probability functions. To this end, we first calculated the equilibrium average and standard deviation (over ∼1 ns) of the potential energy and continuous coordination number for *each* individual atom in the relaxed target. The atom-specific probability functions can then be built; if the properties of a given atom fall beyond a certain "individual" threshold following the passage of the ion, this atom is declared to be suspect—i.e., has potentially been seriously affected by the ion—and is flagged. The flagged atoms, and only those, are then filtered through the probability function defined earlier using the bulk, or "collective," threshold. This procedure ensures that only atoms having been excited, directly or indirectly, by the energetic ion are considered. Indeed, it filters out atoms that may have been in some local minimum of the amorphous state before implantation and that may have moved away from the minimum over time without having been induced into an anomalous state as a result of the collision process: because the relaxed state of a-Si is inherently disordered, an atom can be different from the average bulk state and still be normal.

3. *Comparison of identification methods for c-Si*

An overall probability can be obtained by summing, for each atom of interest, the individual property-specific probabilities. The probability thresholds for declaring an atom to be anomalous are evidently not defined *a priori* and must be chosen with care, an inherent complication of the method. One strategy is to refer to a well-defined method in a simple system—the obvious choice here is to compare the two identification methods for c-Si. Additionally, empirical or heuristic arguments may be invoked. In particular, there should be only a few anomalous atoms in the target before implantation, or in regions so far away that they cannot have been affected by the implantation.

We thus first consider the crystalline target, for which we used a combination of individual threshold = 0.4 and collective threshold = 0.168, yielding no damage before implantation, no randomly appearing, isolated, anomalous atoms after implantation, and most importantly, the same amount of persistent anomalous atoms as of persistent topological defects. The variation of the number of defects with time is presented in Fig. 6 for the two methods. At long times, the proportion of damage in the two approaches is similar (∼300 atoms), suggesting that they are in qualitative agreement when the implanted energy has dissipated in the target. More quantitatively, above 1 ps, 40%–50% of the anomalous atoms actually correspond to topological defects while another 35% have a defect as one of their first neighbors; this is shown by the blue and purple areas in Fig. 6. Hence, in this second regime, which corresponds to the persistent damage regime observed earlier using the topological method, more than 75% of the anomalous atoms correspond to sites strongly influenced by the presence of a topological defect.

Thus, our method is capable of successfully identifying atoms that are in an anomalous state, resulting most of the time from their peculiar local environment. In the persistent regime, the probability is not dominated by a single component: all components (potential energy, CC, bond angle) contribute about equally to the total probability. Recrystallization proceeds by steps, as can be seen in the inset to Fig. 6. A visual inspection of the state of the system confirms that the method also reveals the stepwise nature of the recrystallization process—cf. Figs. 1(b3) and 1(b4). Conversely, in the early regime of damage production (below 1 ps), the probabilistic

approach appears to be significantly more sensitive to damage than the topological approach, yielding a much better contrast with the long-time, permanent damage regime. Very early in the damage-production process, i.e., immediately following implantation, a large number (>1400) of atoms become anomalous. These decay rapidly—60% return to a normal state (that is, below threshold) in ∼4 ps. The higher sensitivity of the probability method during the early regime results from the fact that, in this regime, many atoms are being displaced from their equilibrium position and passing above threshold, thus becoming anomalous. However, they are not yet sufficiently displaced to be removed from their six-member rings, and hence are not flagged as defects by the topological method. This is also visible in the probability components: in this early regime, the total probability is completely dominated by the potential energy component. By design, the probability method is therefore more sensitive to the detailed displacement of the atoms than the topological method. In fact, we could choose threshold values so as to include all topological defects, but this would greatly increase the initial amount of anomalous atoms without significantly affecting the comparison between the two systems, as we will discuss below.

4. Probability method applied to a-Si

We now proceed with a corresponding analysis, using the probability method, for the *a*-Si target. As mentioned earlier, this is delicate because of the natural variations in the values of the topological properties of the system. Even though the collective and individual probabilities self-adjust to the wider range of properties, the main challenge is to properly define the threshold values since we do not dispose of a closely comparable reference in *a*-Si—this is really the heart of the matter. Some simple arguments can, however, be invoked. First, while we do not know if the persistent structural damage should be the same in *a*-Si and *c*-Si, it can safely be anticipated that the *initial* damage should look alike in the two phases because, at high energy, the details of the structure are not expected to be very important. (One exception could be the occurrence of replacement collisions in the crystal, but the probability of such process is very small and thus not a relevant factor in our comparisons.) Second, one would ideally wish the ratio of anomalous atoms in the late and early stages to be optimal, i.e., to maximize the sensitivity. Actually, while the absolute numbers do vary somewhat, the overall picture appears to be relatively insensitive to the specific values of the thresholds: this is illustrated in Fig. 7 where we plot the number of anomalous atoms vs time for different combinations of individual and collective thresholds. The overall behavior of initial damage in all cases resembles that observed in *c*-Si: the rapid production and subsequent relaxation of a large number of anomalous atoms (within about 2.5 ps), followed by a distribution of persistent damage. In practice, we found that the combination of an individual threshold = 0.7 and a collective threshold = 0.002 was adequate, reproducing properly the high-energy regime of target damage while yielding relatively few anomalous atoms before implantation (viz., ∼100). The differences with the threshold values for the crystal (0.4 and 0.168, respectively) reflect the degrees of order of the two systems: in the crystal, the local minimum of each atom is

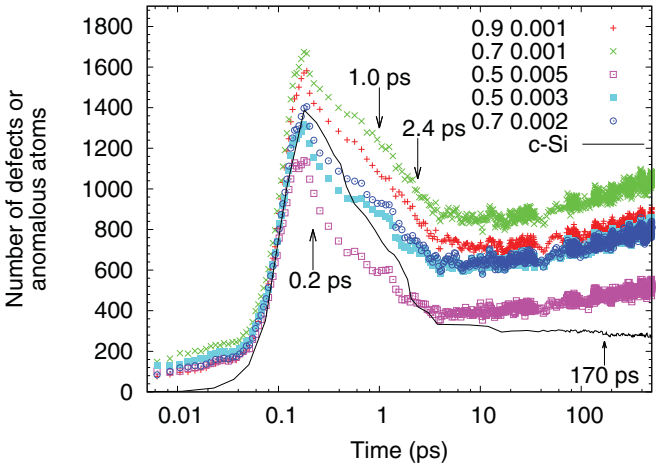

FIG. 7. (Color online) Number of anomalous atoms as a function of time in the *a*-Si target using various individual and collective thresholds.

very precisely defined (i.e., the distribution is narrow) so that any small disturbance yields anomalous atoms if the collective threshold is not sufficiently large. As a final note on this issue, the thresholds must be seen as a tool for pinpointing atoms that are not in their normal state, and identifying regions that have been damaged.

We analyze now the restructuring processes that take place in the first stage of damage production and relaxation, as summarized in Fig. 7. The number of anomalous atoms reaches a maximum at about 0.22–0.26 ps, and this is followed by a rapid descent that seems to level off at $t \sim 2.5$ ps, at the onset of a persistent regime and at which point the number of anomalous atoms begins to *increase* rather than level off or decrease, as is the case in *c*-Si (full black line in Fig. 7). This very significant difference will be discussed shortly. The right column of Fig. 1 presents a sequence of snapshots for this system, at different points in the simulation, indicated by arrows in Fig. 7.

Figure 7 shows that the initial damage inflicted to the *a*-Si target by the energetic ions is, as expected, very similar to that seen in *c*-Si: defects are primarily concentrated in clusters along the ion's trajectory and relaxation (between 0.26 and ∼1.5 ps) proceeds by single-atom annealing events. However, just as there were fewer cluster annealing events in the probability approach vs the topological approach in the case of *c*-Si, Figs. 1(c2) and 1(c3) reveal that cluster annealing is essentially absent in *a*-Si.

The behavior of the persistent damage regime in the two materials is thus inherently different in at least three ways: First, setting equal the short-time behavior of the two phases, the absolute amount of damage appears to be larger in *a*-Si than in *c*-Si; this is related to the fact that *a*-Si has a larger mixing property than *c*-Si, as demonstrated by Nordlund and Averback,[33] and hence more atoms are bound to be affected by the implantation process. This result is also consistent with nanocalorimetry observation of a higher heat release during the annealing of implanted *a*-Si compared to polycrystalline Si.[7] Second, the amount of persistent damage increases in *a*-Si while it decreases in *c*-Si. Third, *a*-Si shows no (or very little) sign of the presence of stepwise

restructuring events (see the inset to Fig. 6), which we have seen correspond to the spontaneous recrystallization of several neighboring anomalous atoms at the surface of clusters. Instead, it can be appreciated from Figs. 1(c1)–1(c4), as well as several other configurations we have examined, that, in *a*-Si, (i) long-term annihilation occurs at random locations as does early annealing and (ii) the damage that was initially concentrated in clusters flows into the rest of the material. For example, in Fig. 1(c4), we find that the anomalous atoms are much more dispersed than in the crystalline phase, and that their number has increased significantly in the regions between the initial clusters.

The increase in the number of anomalous atoms in the persistent damage regime must *not* be interpreted as an increase in the number of defects. It is, rather, a consequence of the long-term flowing and redistribution of the implantation damage: as time passes, the structure evolves from a situation where few atoms satisfy the probability criteria by a relatively large gap to a situation where more atoms satisfy the criteria but with values closer to the threshold. Overall, and in spite of the fact that the number of anomalous atoms increases, the total energy of the system decreases; and of course, at very long times—beyond the scope of our simulations—the number of anomalous atoms would eventually decrease. We have also verified that this effect was not an artifact of our method by simulating the same system without implantation: no random anomalous atom generation was observed on the same time scale.

Thus, rather than annealing by steps through cluster-recrystallization events as is the case in *c*-Si, damage in *a*-Si flows into the bulk of the material by virtue of a process that is likely related to heat diffusion. The increasing number of anomalous atoms conveys the fact that damage is slowly spreading over all the degrees of freedom of the system. In both Si phases, the complexity of the resulting structures translates into a broad range of activation energies for the annealing mechanisms, which itself results in a broad distribution of heat release processes, as observed in nanocalorimetry experiments[7] but, in view of the present results, for different reasons.

IV. CONCLUSION

Using MD simulations, we have studied the formation and evolution of damage caused by keV ion implantation in crystalline and amorphous silicon targets. The defect pockets that result are found to be akin to a compact amorphous phase, and are certainly not liquid. We have presented an approach, based on probabilities for the properties of atoms to be normal or anomalous, for identifying damage in the amorphous material. In the crystal, more than 75% of such anomalous atoms correspond to topological defects—themselves or one of their first neighbors—during the reproduction of the persistent damage regime.

Our study reveals that the initial, high-energy regimes of the two systems behave in a similar manner. On longer time scales, the persistent damage regimes behave differently. In the case of *c*-Si, relaxation proceeds by the stepwise recrystallization of portions of defect clusters at the interface with the crystalline matrix. In *a*-Si, in contrast, the damage caused by the energetic ions, initially compact, spreads out—flows, or percolates—into the system, causing an overall derelaxation. The increasing number of anomalous atoms (notwithstanding the *decrease* of the total energy) indicates that the damage spreads over all degrees of freedom of the system—less severe damage but dispersed over a larger portion of the material. Thus, while *c*-Si and *a*-Si have very similar short-range configurations, the perturbation caused by the implanted ion induces rather different effects owing to the more "sensitive" nature of *a*-Si where a sort of damage percolation is observed. Our calculations provide a simple explanation for nanocalorimetry experiments[7] which indicate that, in both *c*-Si and *a*-Si, the heat released exhibits broad features; the underlying physics is, however, different.

APPENDIX

We provide here some details of the probability functions used in the present work. We first need to adjust the parameters x_0 and σ_0 in Eq. (1), which requires that two points of the function be fixed. As an example, we consider the distribution of angles shown in Fig. 4; the standard deviation σ for this property is given in Table I. The two constraints we impose determine the sensitivity of the function. For the angle and the CC, we set $P(\sigma) \sim 0$ for the first point and $P(4\sigma) = 1/e$ for the second, this last point being just out of the distribution tail on both sides. The energy distribution is much broader than other properties so we set $P(2\sigma) \sim 0$. Furthermore, since we are analyzing three properties, an atom at $P(4\sigma)$ for all properties in the distribution will have a $P_{\text{tot}} = 3/e \sim 1$, thus being 100% anomalous. We give below, for illustration purposes, the set of functions used for the *c*-Si target, viz., for (local) continuous coordination C, angle θ, and energy E:

$$P_{\text{CC}}(C) = 2 - 1/(1 + e^{-(C-3.3)/0.07}) - 1/(1 + e^{-(C-4.7)/-0.07}),$$

$$P_{\text{angle}}(\theta) = 2 - 1/(1 + e^{-(\theta-95.2)/1.6}) - 1/(1 + e^{-(\theta-123.6)/-1.6}),$$

$$P_{\text{energy}}(E) = 1 - 1/(1 + e^{-(E+7.5)/-0.14}).$$

The probability functions are similar for *a*-Si; however, the parameters are system specific and thus need to be calculated for each different target; hence an exhaustive list cannot be provided.

ACKNOWLEDGMENTS

We are grateful to Patrick Lorazo for invaluable help in setting up the computer codes and to Normand Mousseau for providing the reference *a*-Si model. This work has been supported by grants from the Natural Sciences and Engineering Research Council of Canada (NSERC) and the Fonds Québécois de la Recherche sur la Nature et les Technologies (FQRNT). We are grateful to the Réseau Québécois de Calcul de Haute Performance (RQCHP) for generous allocations of computer resources.

*Author to whom correspondence should be addressed: Laurent.Lewis@UMontreal.CA

[1]M. O. Ruault, J. Chaumont, J. M. Penisson, and A. Bourret, Philos. Mag. A **50**, 667 (1984).
[2]L. Howe and M. Rainville, Nucl. Instrum. Methods **182–183**, 143 (1981).
[3]M. Alurralde, F. Paschoud, M. Victoria, and D. Gavillet, Nucl. Instrum. Methods Phys. Res., Sect. B **80–81**, 523 (1993).
[4]K. Nordlund, M. Ghaly, R. S. Averback, M. Caturla, T. Diaz de la Rubia, and J. Tarus, Phys. Rev. B **57**, 7556 (1998).
[5]T. Diaz de la Rubia and G. H. Gilmer, Phys. Rev. Lett. **74**, 2507 (1995).
[6]S. Roorda, W. C. Sinke, J. M. Poate, D. C. Jacobson, S. Dierker, B. S. Dennis, D. J. Eaglesham, F. Spaepen, and P. Fuoss, Phys. Rev. B **44**, 3702 (1991).
[7]R. Karmouch, Y. Anahory, J.-F. Mercure, D. Bouilly, M. Chicoine, G. Bentoumi, R. Leonelli, Y. Q. Wang, and F. Schiettekatte, Phys. Rev. B **75**, 075304 (2007).
[8]K. Laaziri, S. Kycia, S. Roorda, M. Chicoine, J. L. Robertson, J. Wang, and S. C. Moss, Phys. Rev. Lett. **82**, 3460 (1999).
[9]I. Santos, L. A. Marqués, L. Pelaz, P. López, M. Aboy, and J. Barbolla, Mater. Sci. Eng. B **124–125**, 372 (2005).
[10]M.-J. Caturla, T. Díaz de la Rubia, L. A. Marqués, and G. H. Gilmer, Phys. Rev. B **54**, 16683 (1996).
[11]L. A. Marqués, M.-J. Caturla, T. D. de la Rubia, and G. H. Gilmer, J. Appl. Phys. **80**, 6160 (1996).
[12]S. E. Donnelly, R. C. Birtcher, V. M. Vishnyakov, and G. Carter, Appl. Phys. Lett. **82**, 1860 (2003).
[13]X. Urli, C. L. Dias, L. J. Lewis, and S. Roorda, Phys. Rev. B **77**, 155204 (2008).
[14]E. Kim, Y. H. Lee, C. Chen, and T. Pang, Phys. Rev. B **59**, 2713 (1999).
[15]F. H. Stillinger and T. A. Weber, Phys. Rev. B **31**, 5262 (1985).
[16]K. Gärtner, D. Stock, B. Weber, G. Betz, M. Hautala, G. Hobler, M. Hou, S. Arite, W. Eckstein, J. J. Jiménez-Rodríguez *et al.*, Nucl. Instrum. Methods Phys. Res., Sect. B **102**, 183 (1995).
[17]J. Ziegler, J. Biersack, and U. Littmark, *The Stopping and Range of Ions in Solids* (Pergamon Press, New York, 1985).
[18]G. T. Barkema and N. Mousseau, Phys. Rev. Lett. **77**, 4358 (1996).
[19]N. Mousseau and G. T. Barkema, Phys. Rev. E **57**, 2419 (1998).
[20]N. Mousseau and G. Barkema, Comput. Sci. Eng. **1**, 74 (1999).
[21]J. Nord, K. Nordlund, and J. Keinonen, Phys. Rev. B **65**, 165329 (2002).
[22]W. D. Luedtke and U. Landman, Phys. Rev. B **40**, 1164 (1989).
[23]R. L. C. Vink, G. T. Barkema, W. F. van der Weg, and N. Mousseau, J. Non-Cryst. Solids **282**, 248 (2001).
[24]S. Plimpton, J. Comput. Phys. **117**, 1 (1995).
[25]M. P. Allen and D. J. Tildesley, *Computer Simulation of Liquids* (Clarendon Press, New York, 1989).
[26]S. M. Nakhmanson and N. Mousseau, J. Phys.: Condens. Matter **14**, 6627 (2002).
[27]P. Beaucage and N. Mousseau, Phys. Rev. B **71**, 094102 (2005).
[28]M. Ishimaru, K. Yoshida, and T. Motooka, Phys. Rev. B **53**, 7176 (1996).
[29]C. Z. Wang, C. T. Chan, and K. M. Ho, Phys. Rev. B **45**, 12227 (1992).
[30]H. Kallel, N. Mousseau, and F. Schiettekatte, Phys. Rev. Lett. **105**, 045503 (2010).
[31]L. A. Marqués, L. Pelaz, P. López, I. Santos, and M. Aboy, Phys. Rev. B **76**, 153201 (2007).
[32]K. Gartner and B. Weber, Nucl. Instrum. Methods Phys. Res., Sect. B **180**, 274 (2001).
[33]K. Nordlund and R. S. Averback, Appl. Phys. Lett **70**, 3101 (1997).